

Mitochondria participate in chemoresistance to cisplatin in human ovarian cancer cells

Luca X. Zampieri,^{1,§} Debora Grasso,^{1,§} Caroline Bouzin,² Davide Brusa,³ Rodrigue Rossignol,⁴ Pierre Sonveaux^{1,*}

¹Pole of Pharmacology and Therapeutics, Institut de Recherche Expérimentale et Clinique (IREC), Université catholique de Louvain (UCLouvain), Brussels, Belgium. ²IREC imaging platform (2IP), Institut de Recherche Expérimentale et Clinique (IREC), Université catholique de Louvain (UCLouvain), Brussels, Belgium. ³IREC Flow Cytometry and Cell Sorting Platform, Institut de Recherche Expérimentale et Clinique (IREC), Université catholique de Louvain (UCLouvain), Brussels, Belgium. ⁴INSERM U1211, Bordeaux University, Bordeaux, France.

[§]Co-first authors.

***Corresponding author:** Pierre Sonveaux, Pole of Pharmacology and Therapeutics, Institut de Recherche Expérimentale et Clinique (IREC), Université catholique de Louvain (UCLouvain), Avenue Hippocrate 57 box B1.53.09, Brussels, 1200, Belgium. Tel: +32 (0)2 7645267; Email: pierre.sonveaux@uclouvain.be

Running title: Resistance of ovarian cancer to cisplatin

Conflict of interest statement. Authors declare no conflict of interest.

Keywords: Ovarian cancer, chemoresistance, cisplatin, cancer metabolism, mitochondria

Abstract word count: 247/250

Number of Figures: 6

Body text word count: 5,859/6,000

Number of references: 50/50

Abstract

Ovarian cancer is an aggressive disease that affects about 300,000 patients worldwide, with a yearly death count of about 185,000. Following surgery, treatment involves adjuvant or neoadjuvant administration of taxane with platinum compounds cisplatin or carboplatin, which alkylate DNA through the same chemical intermediates. However, although platinum-based therapy can cure patients in a number of cases, a majority of them discontinues treatment owing to side effects and to the emergence of resistance. In this study, we focused on resistance to cisplatin and investigated whether metabolic changes could be involved. As models, we used matched pairs of cisplatin-sensitive (SKOV-3 and COV-362) and cisplatin-resistant (SKOV-3-R and COV-362-R) human ovarian carcinoma cells that were selected *in vitro* following exposure to increasing doses of the chemotherapy. Metabolic comparison revealed that resistant cells undergo a shift towards a more oxidative metabolism. The shift goes along with a reorganization of the mitochondrial network, with a generally increased mitochondrial compartment. More functional mitochondria in cisplatin-resistant compared to cisplatin-sensitive cells were associated to enzymatic changes affecting either the electron transport chain (SKOV-3/SKOV-3-R model) or mitochondrial coupling (COV-362/COV-362-R model). Our findings further indicate that the preservation of functional mitochondria in these cells could be due to an increased mitochondrial turnover rate, suggesting mitophagy inhibition as a potential strategy to tackle cisplatin-resistant human ovarian cancer progression. **Implications:** Besides classical mechanisms related to drug efflux and target modification, we report that preserving functional mitochondria is a strategy used by human ovarian cancer cells to resist to cisplatin chemotherapy.

Introduction

Ovarian cancer is the most lethal genital malignancy and the 5th cause of cancer death among women.^a At stage 1, when the primary tumor is limited to ovaries, cure can be achieved by surgical resection of internal genitals (1). At stages 2 to 4, when the tumor progressively extends to the pelvis, peritoneal tissues, retroperitoneal lymph nodes and extra-abdominal organs, the treatment of choice is cytoreduction followed by platinum/taxane combination chemotherapy, which can be administered in adjuvant and/or neoadjuvant settings. However, relapse is frequent (70% of patients), and recurrent tumors most often develop resistance to chemotherapy, which eventually leads to patient death (2).

Cisplatin is the most commonly used chemotherapeutic drug for the treatment of several types of cancers, including bladder, head and neck, lung, ovarian and testicular cancers. It is administered by intravenous injection as an inactive prodrug that must undergo hydrolysis inside cancer cells to be activated (3). Activated cisplatin is a potent electrophile that can react with nucleophilic biomolecules, cross the nuclear membrane and bind covalently to guanine and adenine in DNA, forming cytotoxic DNA adducts. However, DNA damage-induced cell death is not its only anticancer mechanism. It is indeed estimated that less than 1% of intracellular platinum is bound to nuclear DNA (nDNA), while most of cisplatin interacts with more accessible nucleophilic sites on other molecules, including mitochondrial DNA (mtDNA), RNA, phospholipids, tubulin and cytosolic organelles (4). Cisplatin also acts as a pro-oxidant that can trigger the production of superoxide and other reactive oxygen species (ROS) inside cells, thus activating intrinsic and extrinsic pro-apoptotic pathways (5, 6). Cisplatin binding to

^a <https://www.cancer.org/research/cancer-facts-statistics/all-cancer-facts-figures/cancer-facts-figures-2019.html>

mtDNA further creates adducts that are not repaired as efficiently as in nDNA (7), and damage to mtDNA genes encoding components of the electron transport chain (ETC) can compromise respiration, which subsequently leads to ROS generation (6).

In ovarian cancer, resistance to cisplatin can proceed through multiple mechanisms categorized as pre-, on-, post- and off-target depending on whether they are implemented by cancer cells before nDNA damage, during the phase of damage signaling, during the implementation of the damage response, or independently of the effects of cisplatin on nDNA, respectively (8). Pre-target mechanisms include reduced drug uptake (9), increased drug efflux (10, 11) and drug inactivation (*e.g.* through a direct reaction of cisplatin with glutathione) (12). On-target resistance mechanisms are those that improve cell ability to repair DNA damage or that allow cell replication by ignoring the damage. Post-target resistance mechanisms arise after nDNA damage and affect the ability of the cells to induce cell death. Prevailing events are inactivation of p53 (13) and overexpression of Bcl2 (14). Finally, off-target mechanisms concern the alteration of processes that are not directly activated by cisplatin but are nevertheless able to counteract the toxic effects of the drug. Autophagy, for example, can be increased in drug-resistant ovarian cancers (15).

Recent discoveries in a variety of cancer types suggested an active participation of mitochondria in chemoresistance (16). Therefore, in this study we hypothesized that cisplatin could alter energy metabolism and redox signaling in ovarian cancer cells. To test this hypothesis, we compared the bioenergetics of two pairs of matched cisplatin-sensitive and cisplatin-resistant SKOV-3/SKOV-3-R (17) and COV-362/COV-362-R cells. Our findings reveal that cisplatin-resistant human ovarian cancer cells undergo an oxidative switch that could be related to an increased mitochondrial turnover rate.

Consequently, targeting autophagy in general and mitophagy in particular could be a strategy to control the proliferation of cisplatin-resistant human ovarian cancer cells.

Material and methods

Cells and cell culture

SKOV-3 human ovarian adenocarcinoma cancer cells, originally from the American Type Culture Collection (ATCC catalogue #HTB-77, RRID: CVCL_0532) were a kind gift of Dr. Shoshan (Karolinska Institute, Stockholm) in 2005, and were routinely cultured in RPMI 1640 (Gibco Life Technologies catalogue #61870-036) containing 11 mM glucose, 2 mM Glutamax and supplemented with 10% fetal bovine serum (FBS). COV-362 human ovarian epithelial endometrioid cancer cells (purchased from Sigma-Aldrich in 2018, catalogue #07071910, RRID: CVCL_2420) were routinely cultured in DMEM containing 4.5 g/L glucose and 2 mM Glutamax, and supplemented with 10% FBS. Cisplatin-resistant SKOV-3 (SKOV-3-R) and COV-362 (COV-362-R) cells were obtained by treating wild type SKOV-3 (SKOV-3) and wild type COV-362 (COV-362) cells, respectively, with increasing concentrations of cisplatin (Teva) from 5 μ M to 10 μ M with increments of 1.5 μ M every 72 h (17). After each selection, cells were cultured for minimum of 6 passages and up to 25 passages in the absence of cisplatin to ensure phenotypic stability. Cell authentication was performed at passage 6 with a short tandem repeat (STR) test (GeneMapper, Applied Biosystem). DNA was isolated with a QIAmp DNA kit (Qiagen) and amplified by PCR using the PowerPlex 16 System Promega amplification kit. Fifteen markers (D3S1358, THO1, D21S11, D18S51, Penta E, D5S818, D13S317, D7S820, D16S539, CSF1PO, Penta D, Vwa, D8S1179, TPOX, FGA and amelogenin) were used to obtain the genetic profile (Laboratoire de Biologie

Moléculaire, Cliniques Universitaires St-Luc, Brussels, Belgium). All cell lines were checked for mycoplasma every 2 months using the MycoAlert Plus Mycoplasma Detection Kit from Lonza (a biochemical test that selectively reports on the activity of mycoplasma enzymes, catalogue #LT07-710), according to manufacturer's instructions.

Cell treatment, viability and clonogenicity

Where indicated, cells were treated with the indicated doses of cisplatin, bafilomycin A1, H₂O₂, rotenone, *N*-acetyl-*L*-cysteine (NAC), antimycin A, oligomycin or a combination thereof (all from Sigma-Aldrich). NAC was used as a 72 h pretreatment at a 5 mM concentration, followed by cisplatin treatment as indicated. To bypass glycolysis yet sustaining cell respiration, 4.5 g/L of galactose (Sigma-Aldrich) were added to glucose-deprived RPMI-1640 (Sigma-Aldrich catalogue #R1383) containing 2 mM Glutamax and supplemented with 10% FBS for SKOV-3/SKOV-3-R cells, or glucose-deprived DMEM (Sigma-Aldrich catalogue #D5030) containing 2 mM *L*-glutamine and supplemented with 10% FBS for COV-362/COV-362-R cells, as previously reported (18). For direct counting, cells were washed with PBS after treatment and stained with 0.5% crystal violet in a 10% ethanol solution for 30-60 min, and washed with water. After 24 h of air-drying, 100 µL of methanol were added to each well and incubated for 20 min at room temperature on a bench rocker with a frequency of 20 oscillations per minute. Optical density was measured at 570 nm with a SpectraMax miniMax 300 imaging cytometer (Molecular Devices). Alternatively, cell number was determined using the SpectraMax minimax 300 automatic count on transmitted light images captured at indicated time points. For clonogenic assays, a range of 50 to 1,000 cells was seeded in 6-well plates and allowed to settle overnight. For every experiment, a control plate was seeded to

obtain the plating efficiency (PE). After 48 h of treatment with test compound(s), media were changed with fresh media. After colony formation, cells were fixed and stained with 0.5% crystal violet in a 10% ethanol solution for 30-60 minutes, washed with water, air dried and counted. Results are expressed as surviving fraction (SF), where $SF = \#colonies/PE$.

Tumor growth in mice

All *in vivo* experiments were conducted under approval of the Université catholique de Louvain (UCLouvain) authorities (*Comité d’Ethique Facultaire pour l’Expérimentation Animale*) according to national animal care regulations. Specific authorization was 2016/UCL/MD/018. Mice had access to water and food *ad libitum*. They were randomly assigned to a treatment group. In a first series of experiments (Protocol 1), anesthetized (ketamine/xylazine) 8 weeks-old female Rj:NMRI-Foxn1^{nu/nu} nude mice (Elevage Janvier, RRID: IMSR_TAC:nmrinu) were subcutaneously injected with 10^6 cancer cells (SKOV-3, SKOV-3-R, COV-362 or COV-362-R; one tumor per mouse) in PBS containing 10% growth factor-reduced (GFR) Matrigel (Corning catalogue #L003975). From day +6 after tumor implantation, mice were intraperitoneally injected with cisplatin 3 mg/kg or vehicle every 3 days for 7 times. Tumor size was measured every 2-3 days with an electronic caliper. After reaching a mean tumor volume of 300 mm^3 , mice were sacrificed by cervical dislocation under anesthesia, and tumors were collected for further analyses. In a second series of experiments (Protocol 2), mice were simultaneously injected with 1.5×10^6 SKOV-3 and SKOV-3-R cancer cells in PBS containing 10% GFR-Matrigel in the left and right flanks, respectively. From day +18 after tumor implantation, mice were intraperitoneally injected with cisplatin 3 mg/kg or vehicle every 3 days. Tumor size was

measured every 2-3 days with an electronic caliper. On day +29, mice were sacrificed by cervical dislocation under anesthesia, and tumors were collected for further analyses.

Metabolic assays

Extracellular and intracellular glucose and lactate concentrations were measured using specific enzymatic assays on a CMA600 analyzer, as previously described (19). Glucose consumption and lactate production rates were calculated and normalized by total protein content obtained using the Bio-Rad protein assay. Oxygen consumption rates (OCRs) were determined on a Seahorse XF96 bioenergetic analyzer using the XF cell mito stress kit (Agilent Technologies) according to manufacturer's recommendations. Briefly, for experiments without concomitant cisplatin treatment, 10,000 cells per well were plated on XF96 culture plates 24 h before experiments in RPMI 1640 (SKOV-3 and SKOV-3-R) or DMEM (COV-362 and COV-362-R) medium containing 10% FBS. For experiments with cisplatin treatment, the protocol was similar except that 3,000 to 4,000 cells per well were plated 48 h before experiments, which allowed to obtain the same final confluence than for cisplatin-untreated cells. On the day of analysis, culture media were replaced by DMEM containing 10 mM glucose, 2 mM glutamine, 1.85 g/L NaCl, 3 mg/L phenol red, pH 7.4. Cells were incubated for 1 h in a CO₂-free incubator before analysis. Data were normalized to cell numbers measured right before oximetry using a SpectraMax miniMax 300 imaging cytometer. All other metabolic assays were performed on confluent cells. Intracellular ATP levels were measured using the CellTiter-Glo luminescent viability assay (Promega) on a Glomax 96 microplate luminometer (Promega) following manufacturer's instructions. Intracellular

succinate was quantified using a succinate colorimetric assay kit (Sigma-Aldrich) following manufacturer's instructions.

Respirometry

Oxygen flow per cell was analyzed using an O2k-respirometer (Oroboros Instrument), according to manufacturer's instructions. Briefly, one million confluent cells per mL were analyzed over time, and the following drugs were sequentially used: oligomycin, CCCP (increasing doses from 100 nM up to plateau), antimycin A and rotenone. The O₂ flow was assessed after each treatment.

Immunocytochemistry

Cells cultured on glass coverslips were fixed in 4% formaldehyde, permeabilized with 0.1% Triton X-100 in PBS containing 0.1% Tween 20, and blocked with 5% bovine serum albumin (BSA). Immunostaining was then performed as previously described (20). Primary antibodies were a rabbit polyclonal against mitochondrial import receptor subunit TOMM20 (Invitrogen catalogue #PA5-52843, RRID: AB_2648808) and a mouse monoclonal against p62 (Santa Cruz catalogue #sc-28359, RRID: AB_628279). Secondary antibodies were an Alexa Fluor 488-conjugated goat anti-rabbit (Invitrogen catalogue #A-11034, RRID: AB_2576217) and an Alexa Fluor 594-conjugated goat anti-mouse (Thermo Fisher Scientific catalogue #A-11005, RRID: AB_141372). Nuclei were stained with 4',6-diamidino-2-phenylindole dihydrochloride (DAPI, 1 µg/mL, Sigma-Aldrich). Cells were counted in 28 different random fields. Images of mitochondria were captured by structured illumination fluorescence microscopy using an ApoTome-equipped AxioImager.z1 microscope (Zeiss). Mitochondrial surface and network

analyses were performed using the ImageJ software (NIH) following a previously described methodology with the MINA plugin (21). Co-localization of mitochondria and p62 was quantified using the AxioVision software (Zeiss).

mtDNA content

mtDNA copy number was determined following the procedure detailed in (22). Briefly, total DNA was isolated with a QIAmp DNA kit (Qiagen) following manufacturer's instructions. RT-qPCR was performed using TaqMan Universal Master Mix II with UNG (Applied Biosystems) on a ViiA 7417 real-time instrument (Life Technologies). nDNA was quantified using the RNaseP VIC 2'-chloro-7'phenyl-1,4-dichloro-6-carboxy-fluorescein-labeled probe (ThermoFisher Scientific). mtDNA was quantified using as primers: forward: 5'-GTA CCC ACG TAA AGA CGT TAG G-3'; reverse: 3'-TAC TGC TAA ATC CAC CTT CG-5'; and as labeled probe 5'-CCC ATG AGG TGG CAA GAA AT-3' FAM 5(6)-carboxyfluorescein. mtDNA content was normalized to nDNA content, as previously done (23).

Cell cycle and polyploidy

Cells at about 30% of confluence were synchronized overnight in RPMI 1640 supplemented with 0.1% FBS, then cultivated in RPMI 1640 supplemented with 10% FBS for a time equivalent to their doubling time. After synchronization, cells were treated with 10 μ M of cisplatin for 24 to 96 h, trypsinized, centrifuged at 500 G and washed twice with PBS. Cells were then fixed by adding 700 μ L of ice-cold ethanol 100% in 300 μ L of cell suspension in PBS. Cells were then washed twice with 1 mL of Tris buffer with Triton X-100 0.2% v/v (TST), and finally resuspended in 300 μ L of PBS with RNase (0.2

mg/mL) and propidium iodide (5 µg/mL). At least 20,000 to 30,000 events were recorded using a BD FACSCalibur flow cytometer. The FlowJo cell cycle analysis tool (BD) was used to interpret data according to DNA content. Polyploidy was analyzed using flow cytometry after propidium iodide staining according to the DNA content per cell.

Determination of cisplatin-DNA adducts

Cisplatin-DNA adducts were quantified using the rat monoclonal antibody CP9/19 targeting cisplatin-modified DNA (Abcam catalogue #ab103261, RRID: AB_10715243) according to manufacturer's recommendations. Briefly, cells at 50% of confluence were cultured for 48 h ± cisplatin, detached with trypsin 0.5% in PBS, fixed with ice-cold ethanol 100% in 300 µL of cell suspension in PBS, and permeabilized with Triton x-100 0.1% in PBS for 10 min on ice. They were then incubated for 18 h with the anti-cisplatin-modified DNA antibody, washed with PBS, and incubated with Alexa Fluor 488 donkey anti-rat IgG secondary antibody (ThermoFisher Scientific catalogue #A-21208, RRID: AB_2535794). The fluorescence intensity of FITC was measured using a BD FACSCanto II flow cytometer, and at least 20,000 events were recorded in each sample. Results were analyzed with FlowJo.

ROS measurements

ROS levels were determined using CM-H₂DCFDA (Invitrogen) freshly prepared by dissolution in DMSO. Briefly, culture medium was removed, and 10,000,000 cells were washed with PBS for 10 min. Cells were resuspended in pre-warmed PBS containing 1 µM of CM-H₂DCFDA and incubated for 45 min. Cells were then washed with PBS, and incubated in complete medium for 15 min to allow the dye to respond to oxidation. H₂O₂

(50 μ M) was used as a positive control. Fluorescence intensity was measured using a BD FACSCanto II flow cytometer, and at least 10,000 events were recorded in each sample.

Western blotting

Western blotting was performed as previously described (24). Primary antibodies were a rabbit polyclonal against LC3 (MBL international catalogue #PD014, RRID: AB_843283) and a mouse monoclonal against β -actin (Sigma-Aldrich catalogue #A5441, RRID: AB_476744). Secondary antibodies were a HRP-coupled goat anti-rabbit (Jackson ImmunoResearch catalogue #AB2307391, RRID: AB_2307391) and anti-mouse (Jackson ImmunoResearch catalogue #115-035-003, RRID: AB_10015289). Staining was revealed with an Amersham Imager 600 (GE Healthcare). Data were analyzed using the ImageJ software.

Statistics

All data are expressed as means \pm SEM. Note that error bars are sometimes smaller than symbols. n refers to the total number of replicates and N to the number of independent experiments per condition. Data were analyzed using GraphPad Prism 7.0. Survival curve fitting was performed using Matlab. Student's t test, one-way ANOVA and two-way ANOVA were used where appropriate. $P < 0.05$ was considered to be statistically significant.

Results

Production of cisplatin-resistant human ovarian cancer cells

To characterize metabolic changes associated to cisplatin chemoresistance in ovarian cancer, we selected SKOV-3 and COV-362 human ovarian adenocarcinoma cancer cells as a models. Cisplatin-resistant SKOV-3-R cells were previously generated by treating SKOV-3 cells with increasing doses of cisplatin (17). We applied the same selection protocol to generate cisplatin-resistant COV-362-R from COV-362 human ovarian epithelial endometroid cancer cells. After selection, cells were cultured for 3 to 6 weeks in the absence of cisplatin to ensure phenotypic stability.

To test their resistance, SKOV-3 and SKOV-3-R cells were challenged with increasing doses of cisplatin. As expected, direct cell count after 24 h or 48 h of treatment showed that SKOV-3-R were significantly more resistant than SKOV-3 cells to doses of cisplatin ranging from 10 μ M to 50 μ M (**Figure 1A**). Doses above 4 μ M of cisplatin for 48 h completely inhibited the clonogenicity of SKOV-3, whereas about 10% of SKOV-3-R cells were still clonogenic at 10 μ M of the drug (**Figure 1B left**). LC50s were \sim 270 nM and \sim 1.86 μ M of cisplatin for SKOV-3 and SKOV-3-R cells, respectively (**Figure 1B right**). Similarly, compared to COV-362, COV-362-R cells were more resistant to increasing doses of cisplatin (**Figure 1C**) and more clonogenic (**Figure 1D left**). LC50s were \sim 7 nM and \sim 110 nM of cisplatin for COV-362 and COV-362-R cells, respectively (**Figure 1D right**).

We next examined cell recovery. Cells were treated for 48 h \pm 10 μ M of cisplatin, washed, and cultured for increasing periods of time in drug-free medium. Although all cell types did recover in this assay, direct cell counting revealed that SKOV-3 were significantly slower than SKOV-3-R cells to repopulate (**Figure 1E left**), and COV-362-R were significantly slower than COV-362 cells to repopulate (**Figure 1E right**). Of important note, untreated SKOV-3 and SKOV-3-R cells proliferated at the same rate,

indicating that chemoresistance to cisplatin did not result from an altered cell proliferation rate in this model. Untreated COV-362-R cells proliferated faster than COV-362 cells. Together, these first sets of data validated SKOV-3/SKOV-3-R and COV-362/COV-362-R as isogenic models to study the metabolic determinants of cisplatin chemoresistance in human ovarian cancer cells *in vitro*.

In mice, using Protocol 1 (see Materials and Methods), SKOV-3 cells (10^6 in GFR-Matrigel) generated fast-growing tumors (**Figure 1F left**). SKOV-3-R cells also generated fast-growing tumors, but tumor engraftment was delayed. Despite a trend for SKOV-3 ($P = 0.085$), tumors generated with either SKOV-3 or SKOV-3-R cells were insensitive to a clinically relevant treatment of 7 cycles of 3 mg/kg of cisplatin every 3 days (25), starting on day +6 post implantation, as shown by tumor doubling times analyzed from the time when tumors reached 100 mm^3 (**Figure 1F right**). Using the same implantation protocol, COV-362 and COV-362-R cells did not generate tumors in the lifetime of immunodeficient mice. We concluded that, compared to the *in vitro* situation, additional parameters influenced the response to cisplatin *in vivo*.

To address this concern, we repeated the experiment using Protocol 2, where mice were simultaneously implanted with SKOV-3 and SKOV-3-R cells (1.5×10^6 cells in GFR-Matrigel) in the left and right flanks, respectively. To avoid interfering with tumor implantation, the treatment was started on day +18 after implantation. Using this experimental protocol, SKOV-3 tumors were found to be sensitive to the clinically relevant treatment of 3 mg/kg of cisplatin every 3 days, as shown by tumor doubling times analyzed from the time when tumors reached 400 mm^3 (**Figure 1G**). Comparatively, SKOV-3-R cells did not generate tumors in the lifetime of the animals, irrespectively of the treatment with cisplatin.

Cisplatin-resistant human ovarian cancer cells are more oxidative than matched cisplatin-sensitive cells

Both models were characterized metabolically using a variety of standardized biochemical assays. Compared to SKOV-3, SKOV-3-R cells consumed more glucose and produced more lactate, indicating accelerated glycolysis (*i.e.*, glycolysis coupled to lactic fermentation), but the lactate/glucose ratio revealed no change in the glycolytic yield (**Figure 2A**). SKOV-3-R cells also had a higher respiratory spare capacity, as revealed under uncoupled conditions (**Figure 2B**). In the second model, COV-362-R had a similar rate of glucose consumption compared to COV-362 cells but produced less lactate, yet the lactate/glucose ratio was unaltered ($P = 0.0671$, **Figure 2C**). COV-362-R cells also had an increased oxygen consumption rate (OCR) and a higher respiratory spare capacity (**Figure 2D**). These findings indicated that cisplatin-resistant human ovarian cancer cells have a better capacity to perform oxidative phosphorylation (OXPHOS) than matched cisplatin-sensitive cells.

To study the molecular mechanisms underpinning the observed oxidative switch, we further investigated OXPHOS. In the SKOV-3 model, enzymatic measurements revealed that the maximal activity of ETC Complex I was highly significantly ($P < 0.001$) increased in SKOV-3-R compared to SKOV-3 cells, while the activities of Complexes II, III and IV were unchanged (**Figure S1A left**). Accordingly, upon Complex I inhibition with 500 nM of rotenone, the OCR of SKOV-3-R was better preserved than that of SKOV-3 cells (**Figure S1B**). Conversely, succinate, which donates electrons to Complex II, was similarly abundant in SKOV-3-R compared to SKOV-3 cells (**Figure S1C**). These observations explain, at least in part, the increased respiratory spare capacity of SKOV-

3-R *versus* SKOV-3 cells. Comparatively, in the COV-362 model, there were no significant changes in the activities of ETC complexes (**Figure S1A right**), OCR sensitivity to rotenone (**Figure S1B**) and succinate levels (**Figure S1C**) when comparing sensitive to resistant cells. However, respiration coupled to OXPHOS (**Figure S1D**) and citrate synthase activity (**Figure S1E**) were increased in COV-362-R cells. These observations explain, at least in part, the increased OCR and respiratory spare capacity of COV-362 *versus* COV-362-R cells. Of note, succinate levels were higher in COV-362 and COV-362-R compared to SKOV-3 cells (**Figure S1C**), further supporting a better respiration coupled to OXPHOS in the former cells.

To evaluate whether the observed increased OXPHOS capacity of resistant cells could be mobilized upon treatment, we measured cell respiration following acute exposure to cisplatin. Cisplatin activated both basal respiration and the spare capacity of SKOV-3-R (**Figure 2E**) and COV-362-R (**Figure 2F**) cells, but at different concentrations (10 μ M and 5 μ M, respectively), which may reflect the different sensitivities of the cells to the drug (**Figure 1A-D**). At 10 μ M of cisplatin, the OCR of COV-362 and COV3-62-R cells went back to that of the corresponding untreated cells, still remaining significantly higher in COV-362-R *versus* COV-362 cells (**Figure 2F**). These findings suggested that cisplatin-resistant cells could potentially exploit OXPHOS to resist to the treatment.

Cisplatin alters the mitochondrial organization of human ovarian cancer cells

One determinant of mitochondrial functions and OXPHOS capacity is organelle dynamics (26), so we examined mitochondrial morphology in our cell models.

For the SKOV-3/SKOV-3-R pair, representative pictures are shown in **Figure 3A**, where mitochondria are labeled in green (TOMM20 staining) and nuclei in blue (DAPI).

In untreated conditions, we detected no difference in the number of individual mitochondria (**Figure 3B**), in the number of mitochondrial tubules (**Figure 3C**) nor in the total mitochondrial area (**Figure 3D**) per cell. Conversely, mtDNA normalized to nDNA content was decreased in SKOV-3-R compared to SKOV-3 cells (**Figure 3E**), while nDNA content per cell was unchanged (**Figure S2A**). When present for 48 h, cisplatin (10 μ M) significantly increased the number of individual mitochondria (**Figure 3B**) as well as the mitochondrial surface (**Figure 3D**) per cell in SKOV-3-R cells. It had no effects on SKOV-3 cells. Polyploidy was increased only in SKOV-3 cells (**Figure S2B**).

For the COV-362/COV-362-R pair, representative pictures are shown in **Figure 3F**. In untreated conditions, COV-362-R had more individual mitochondria (**Figure 3G**), more mitochondrial networks (**Figure 3H**) and an increased mitochondrial surface (**Figure 3I**) per cell compared to COV-362 cells. mtDNA normalized to nDNA content was unchanged (**Figure 3J**). Cisplatin (10 μ M) incubated for 48 h significantly increased the mitochondrial surface per cell in COV-362 cells (**Figure 3I**), while the number of individual mitochondria (**Figure 3G**) and the number of mitochondrial networks (**Figure 3H**) were unchanged. The number of individual mitochondria (**Figure 3G**) and the number of mitochondrial networks (**Figure 3H**) were further increased by cisplatin in COV-362-R cells, while the mitochondrial surface did not change (**Figure 3I**).

Together, these observations indicated that resistance to cisplatin was associated to fitter (*i.e.*, less abundant yet more functional) mitochondria in our models, but for different reasons. Compared to matched sensitive cells, SKOV-3-R cells had more oxidative mitochondria due to increased Complex I activity (**Figure S1A-B**) while mitochondrial organization was largely preserved (**Figure 3A-E**), and COV-362-R cells

had more oxidative mitochondria due to an increased coupling between respiration and OXPHOS (**Figure S1C-E**), with more abundant mitochondria (**Figure 3F-J**).

Neither altered OXPHOS, glycolysis, cisplatin-induced DNA damage nor antioxidant defenses account for cisplatin resistance in human ovarian cancer cells

We then tested whether increased OXPHOS was a cause or a consequence of resistance to cisplatin. Inhibiting cell respiration with ETC Complex III inhibitor antimycin A (500 nM) was more cytotoxic for SKOV-3-R than for SKOV-3 cells (**Figure S3A**). However, the opposite was observed in the COV-362/COV-362-R model (**Figure S3B**). Inhibiting OXPHOS with ATP synthase inhibitor oligomycin (1 μ M) in SKOV-3 and SKOV-3-R cells (**Figure S3C left**) and in COV-362 and COV-362-R cells (**Figure 3D left**) was similarly effective in sensitive *versus* resistant cells, and resulted in an increased glycolytic rate reflected by an increased 2-deoxyglucose-sensitive (2-DG) extracellular acidification rate (ECAR) (**Figures S3C-D middle left**). Oligomycin alone was not significantly cytotoxic for any of the cell types (**Figure S3C-D middle right**). However, it increased the cytotoxicity of cisplatin (10 μ M) in both sensitive and resistant cells (**Figure S3C-D right**). Inhibiting OXPHOS can thus sensitize human ovarian cancer cells to cisplatin, but without discriminating sensitive and resistant cells.

We also tested a potential contribution of glycolysis to cisplatin chemoresistance. SKOV-3 and SKOV-3-R cells cultured in the presence of galactose instead of glucose (18) experienced a decreased 2-DG-sensitive ECAR (**Figure S3E middle**), indicating a reduced glycolytic metabolism. OCR was slightly reduced in SKOV-3 but not in SKOV-3-R cells (**Figure SE3 left**). The treatment was cytostatic (**Figure S3E right**). SKOV-3 cells

kept their sensitivity to cisplatin (10 μ M) and SKOV-3-R cells were still resistant to the chemotherapy. Similar effects were seen in COV-362 and COV-362-R cells, except that galactose was less efficient than glucose to sustain the high basal OCR of COV-362-R cells (**Figure S3F**).

Because modulating ETC activity, OXPHOS and glycolysis had no specific effects on cisplatin-resistant cells, the link between metabolism and resistance could be more subtle, the reason why we inspected the cell cycle, focusing on the SKOV-3/SKOV-3-R model. Exposure of the cells to cisplatin (10 μ M) induced an S-phase arrest in SKOV-3 but not in SKOV-3-R cells (**Figure 4A**). This could be due to direct or indirect effects of cisplatin, or to altered DNA repair mechanisms.

Using specific antibodies to detect cisplatin adducts on DNA, we observed that cisplatin (10 μ M, 48 h) induced similar DNA damage in SKOV-3 *versus* SKOV-3-R and in COV-362 *versus* COV-362-R cells (**Figure 4B**), indicating that cisplatin equally reached its DNA target in sensitive and resistant cancer cells.

Cancer cell killing by cisplatin also depends on cisplatin-induced ROS production (5, 6). Interestingly, basal ROS production was higher in SKOV-3-R compared to SKOV-3 cells (**Figure 4C**). We therefore envisioned that increased basal ROS levels could prime antioxidant defenses in resistant cells. However, challenging the cells with 5 mM H₂O₂ for 48 h did not spare SKOV-3-R compared to SKOV-3 cells (**Figure 4D**). Conversely, pretreating the cells for 24 h or 48 h with 5 mM of glutathione analogue *N*-acetyl-L-cysteine (NAC) did not modulate the cytotoxicity of cisplatin (**Figure 4E**). It increased rather than decreased the clonogenicity of cisplatin-treated SKOV-3, with no significant effects on SKOV-3-R cells (**Figure 4F**). Overall, we concluded that resistance to

cisplatin was not linked to an alteration of cisplatin-induced DNA damage nor to altered antioxidant defenses in human ovarian cancer cells.

Cisplatin-resistant human ovarian cancer cells rely on mitophagy and can be targeted by inhibiting autophagy

Finally, we aimed to understand why cisplatin-resistant ovarian cancer cells had fitter mitochondria compared to their cisplatin-sensitive counterparts. We hypothesized that resistant cells could recycle mitochondria faster. Indeed, compared to SKOV-3, SKOV-3-R cells had a higher basal content in LC3-I (**Figure 5A**), *i.e.*, the precursor form of LC3-II associated with both autophagy and mitophagy (27). Upon cisplatin-treatment, the expression of both LC3-I and LC3-II was increased in SKOV-3-R, while it was unchanged in SKOV-3 cells, and the ratio LC3-II/LC3-I was increased as well (**Figure 5A**).

To discriminate between halted *versus* increased autophagy and to test the biological significance of these observations, we blocked autophagy using bafilomycin A1 (10 nM), and inspected the colocalization of mitochondria with p62, based on the fact that p62 interacts with mitochondria to address them to mitophagic degradation (28). Bafilomycin caused the accumulation of p62-labeled mitochondria in SKOV-3-R but not in SKOV-3 cells (**Figure 5B**), and mtDNA accumulated (**Figure S4**). Similar results were found in COV-362-R compared with COV-362 cells (**Figure 5C**), suggesting that cisplatin-resistant ovarian carcinoma cells could rely on mitophagy more heavily than their cisplatin-sensitive counterparts.

Autophagy can be increased in cisplatin-resistant ovarian cancers (15), and inhibiting autophagy is a promising anticancer strategy (29). Accordingly, we observed

that low doses of bafilomycin A1 (5 to 10 nM) highly significantly repressed SKOV-3-R (**Figure 6A**) and COV-362-R (**Figure 6B**) cell expansion *in vitro*. However, similar effects were seen in SKOV-3 and COV-362 cells (**Figure 6A-B**). When used in combination, cisplatin (10 μ M) and bafilomycin A1 (10 nM) had additive effects on the number of SKOV-3-R but not on the number of SKOV-3 cells (**Figure 6C left**). Comparatively, additive effects of the two treatments were observed both in COV-362-R and in COV-362 cells (**Figure 6C right**). Interestingly, bafilomycin A1 inhibited the clonogenicity of SKOV-3 cells by ~90% and the clonogenicity of SKOV-3-R cells by ~99%, thus showing selectivity for cisplatin-resistant cells (**Figure 6D left**), which was confirmed for COV-362-R compared to COV-362 cells (**Figure 6D right**).

Together, these data indicated that autophagy/mitophagy supports the clonogenicity of human ovarian cancer cell, preferentially cisplatin-resistant cells. Our data thus support the future evaluation of mitophagy inhibition as a potential treatment for cisplatin-resistant ovarian cancers.

Discussion

The main finding of this study is that acquired resistance to cisplatin by human ovarian cancer cells is associated to an oxidative switch relying on enhanced mitochondrial preservation after treatment. Consequently, targeting cell respiration (with antimycin A or oligomycin) or autophagy/mitophagy (with bafilomycin A1) were identified as efficient strategies to control the proliferation of cisplatin-resistant cells. Among these treatments, only autophagy/mitophagy inhibition was more efficient to reduce the clonogenicity of cisplatin-resistant compared to cisplatin-sensitive cells, thus showing some selectivity.

While many mechanisms (detailed in the introduction) can account for resistance to cisplatin in ovarian cancer, our main objective in this study was to identify metabolic changes associated to resistance and simultaneously present in two independent experimental cell models. In cisplatin-resistant cancer cells, we identified a common switch to a more oxidative metabolism, which was further stimulated by acute exposure to cisplatin. The switch proceeded through different molecular changes involving either an increased activity of ETC Complex I or improved coupling between the ETC and OXPHOS. Interestingly, SKOV-3-R cells also had an increased glycolytic metabolism (*i.e.*, glycolysis coupled to lactic fermentation), but this was not shared by the second model. Bypassing glycolysis by replacing glucose by galactose (18) was cytostatic, but it did not chemosensitize cisplatin-resistant cancer cells, indicating that previously reported attempts to re-sensitize ovarian cancer cells to cisplatin *via* inhibition of glycolysis (30, 31) might be only applicable to a limited number of cases. This proposition is supported by Dar S *et al.* (32) who analyzed 13 established and 12 patient-derived ovarian cancer cell lines, reporting high metabolic heterogeneity in general, but a preferential dependency on glycolysis for cisplatin-sensitive cells and on OXPHOS for cisplatin-resistant ones. Xu Y *et al.* (30) further reported a correlation between high Bcl2 expression and elevated OXPHOS in cisplatin-resistant SKOV3/DDP, another resistant variant of SKOV-3 cells. OCR was higher in resistant *versus* sensitive patient-derived xenografts. Consequently, metformin (inhibiting ETC Complex I) (33), antimycin A (inhibiting ETC Complex III; our study) and oligomycin (inhibiting ATP synthase; our study) efficiently killed cisplatin-resistant human ovarian cancer cells. However, these treatments were not selective, as sensitive cancer cells died as well.

Although we here provide molecular explanations for the oxidative switch in resistant cells, the biological significance of the switch was obscure. High OXPHOS activities inevitably increase electron leak from the ETC, hence mitochondrial superoxide production, and mtROS can promote tumor aggressiveness by stimulating protumoral signaling pathways and/or by priming antioxidant defenses (mitohormesis) (34). However, neither targeting ROS (with NAC) nor challenging antioxidant defenses (with H₂O₂) re-sensitized our resistant cells to cisplatin. Moreover, we found no change of cell proliferation that could have accounted for chemoresistance. However, in our models, the *in vitro* selection of resistance to cisplatin was associated to increased clonogenicity and delayed tumor take in mice. These characteristics are shared by ovarian cancer stem cells (CSCs), which also have a higher rate of OXPHOS (35, 36) and are more resistant to cisplatin (37, 38) than non-CSCs. Whether treating cancer cells with increasing doses of cisplatin selects CSCs certainly warrants further investigation.

Interestingly, fitter mitochondria (*i.e.*, more active yet less abundant) in cisplatin-resistant cells were also better preserved following acute treatment with cisplatin, with generally better networking and an increased surface compared to sensitive cells. Comparatively, cisplatin equally reached the nuclear compartment in both cases, producing similar nDNA damage in sensitive and resistant cells. Nevertheless, a S-phase cell cycle blockade was bypassed by resistant cells, indicating a different DNA damage repair strategy in SKOV-3 *versus* SKOV-3-R cells.

Based on our data, we propose that cisplatin-resistant ovarian cancer cells have a faster mitochondrial turnover rate. This hypothesis is supported by the highly significant increase in p62-labeled mitochondria upon autophagy blockade in our resistant cells, suggesting elevated mitophagy, while mtDNA content was preserved, suggesting

elevated mitochondrial biogenesis. Comparatively, sensitive cells did not show this profile. Others reported increased mitochondrial biogenesis and fusion in cisplatin-treated resistant ovarian cancer cells (39-42). For treatment, a further discrimination between autophagy and mitophagy was not necessary, as several previous studies correlated cisplatin-resistance in ovarian cancer cells with a high rate of autophagy (31, 43-47), and bafilomycin A1 almost equally efficiently killed both cisplatin-sensitive and cisplatin-resistant ovarian cancer cells. However, clonogenic assays revealed a more intense inhibitory effect of bafilomycin A1 on cisplatin-resistant cells, which we believe could be linked to an enrichment in stem cell features in our selection protocol. Accordingly, an increased autophagic rate is a characteristic of ovarian CSCs (47, 48), calling for a future examination of the contribution mitochondrial turnover to the oxidative profile of CSCs in this type of cancer.

A limitation of our study is that the chemosensitive/chemoresistant phenotypes that we selected *in vitro* was partially lost *in vivo*. Indeed, if in a first series of experiments the increased time for tumor take in mice for SKOV-3-R compared to SKOV-3 cells was an evident difference between the two variants, tumors turned out to be equivalently insensitive to a clinically relevant regiment of cisplatin (7 cycles of 3 mg/kg of cisplatin every 3 days) (25). While tumors formed from resistant cells remained resistant, those formed from sensitive cells were resistant as well. It suggested that, compared to the *in vitro* situation where culture parameters are well controlled, several pathways supporting cisplatin-resistance are potentially activated under the influence of the *in vivo* tumor microenvironment (e.g. suboptimal tumor perfusion, hypoxia, acidosis). In this context, it is interesting to note that hypoxia stimulates autophagy in ovarian cancers in mice (49, 50), which calls for a systematic evaluation of interventions targeting

autophagy/mitophagy in ovarian cancer models in mice. While these considerations stay valid, a second series of experiments showed that, if the treatment was started later after tumor implantation, SKOV-3 cells retained sensitivity to cisplatin *in vivo*, indicating that cisplatin could also interfere with the early stages of tumor development in this model.

In summary, our study used matched cisplatin-sensitive and cisplatin-resistant human ovarian cancer cells that were metabolically compared. Our data support that resistant cells undergo metabolic reprogramming to an ovarian CSC-like phenotype characterized by increased OXPHOS, mitochondrial turnover and autophagy. While cisplatin-resistant cells were sensitive to OXPHOS and autophagy/mitophagy inhibition, further studies are needed to firmly establish their CSC nature.

Acknowledgments

This work was supported by European Union's Horizon 2020 research innovation program under the Marie Skłodowska-Curie grant agreements No 722605 TRANSMIT and No 642623 RADIATE, the Belgian *Fonds National de la Recherche Scientifique* (F.R.S.-FNRS, CDR J.0135.18), the Belgian Télévie (project n°7.4617.17) and the UCLouvain *Bourses du Patrimoine*. LX Zampieri is a PhD Fellow of Marie Skłodowska-Curie grant No 722605 TRANSMIT. D Grasso is a PhD Fellow of Marie Skłodowska-Curie grant No 642623 RADIATE, a PhD Fellow of the Télévie and was supported by an UCLouvain *Bourses du Patrimoine*. P Sonveaux is a F.R.S.-FNRS Senior Research Associate. Authors thank Maria Shoshan (Karolinska Institute, Stockholm, Sweden) for the kind gift of SKOV-3 and SKOV-3-R cells; Thibaut Vazeille, Loïc Hamelin, Marie Bedin and Elodie Dumon for excellent technical assistance; and Vincent Haufroid at the Louvain Center for Toxicology and Applied Pharmacology (LTAP, UCLouvain).

References

- (1) Trimbos JB. Surgical treatment of early-stage ovarian cancer. *Best Pract Res Clin Obstet Gynaecol* 2017;41:60-70.
- (2) de Jongh FE, van Veen RN, Veltman SJ, de WR, van der Burg ME, van den Bent MJ, et al. Weekly high-dose cisplatin is a feasible treatment option: analysis on prognostic factors for toxicity in 400 patients. *Br J Cancer* 2003;88:1199-206.
- (3) Takahara PM, Rosenzweig AC, Frederick CA, Lippard SJ. Crystal structure of double-stranded DNA containing the major adduct of the anticancer drug cisplatin. *Nature* 1995;377:649-52.
- (4) Makovec T. Cisplatin and beyond: molecular mechanisms of action and drug resistance development in cancer chemotherapy. *Radiol Oncol* 2019;53:148-58.
- (5) Berndtsson M, Hagg M, Panaretakis T, Havelka AM, Shoshan MC, Linder S. Acute apoptosis by cisplatin requires induction of reactive oxygen species but is not associated with damage to nuclear DNA. *Int J Cancer* 2007;120:175-80.
- (6) Marullo R, Werner E, Degtyareva N, Moore B, Altavilla G, Ramalingam SS, et al. Cisplatin induces a mitochondrial-ROS response that contributes to cytotoxicity depending on mitochondrial redox status and bioenergetic functions. *PLoS ONE* 2013;8:e81162.
- (7) Olivero OA, Chang PK, Lopez-Larraza DM, Semino-Mora MC, Poirier MC. Preferential formation and decreased removal of cisplatin-DNA adducts in Chinese hamster ovary cell mitochondrial DNA as compared to nuclear DNA. *Mutat Res* 1997;391:79-86.
- (8) Galluzzi L, Senovilla L, Vitale I, Michels J, Martins I, Kepp O, et al. Molecular mechanisms of cisplatin resistance. *Oncogene* 2012;31:1869-83.

- (9) Li T, Peng J, Zeng F, Zhang K, Liu J, Li X, et al. Association between polymorphisms in CTR1, CTR2, ATP7A, and ATP7B and platinum resistance in epithelial ovarian cancer. *Int J Clin Pharmacol Ther* 2017;55:774-80.
- (10) Nakayama K, Kanzaki A, Ogawa K, Miyazaki K, Neamati N, Takebayashi Y. Copper-transporting P-type adenosine triphosphatase (ATP7B) as a cisplatin based chemoresistance marker in ovarian carcinoma: comparative analysis with expression of MDR1, MRP1, MRP2, LRP and BCRP. *Int J Cancer* 2002;101:488-95.
- (11) Januchowski R, Sterzynska K, Zaorska K, Sosinska P, Klejewski A, Brazert M, et al. Analysis of MDR genes expression and cross-resistance in eight drug resistant ovarian cancer cell lines. *J Ovarian Res* 2016;9:65.
- (12) Chen HH, Kuo MT. Role of glutathione in the regulation of Cisplatin resistance in cancer chemotherapy. *Met Based Drugs* 2010;2010.
- (13) Gadducci A, Cosio S, Muraca S, Genazzani AR. Molecular mechanisms of apoptosis and chemosensitivity to platinum and paclitaxel in ovarian cancer: biological data and clinical implications. *Eur J Gynaecol Oncol* 2002;23:390-6.
- (14) Risnayanti C, Jang YS, Lee J, Ahn HJ. PLGA nanoparticles co-delivering MDR1 and BCL2 siRNA for overcoming resistance of paclitaxel and cisplatin in recurrent or advanced ovarian cancer. *Sci Rep* 2018;8:7498.
- (15) Wang J, Wu GS. Role of autophagy in cisplatin resistance in ovarian cancer cells. *J Biol Chem* 2014;289:17163-73.
- (16) Patel TH, Norman L, Chang S, Abedi S, Liu C, Chwa M, et al. European mtDNA variants are associated with differential responses to cisplatin, an anticancer drug: implications for drug resistance and side effects. *Front Oncol* 2019;9:640.

- (17) Wintzell M, Lofstedt L, Johansson J, Pedersen AB, Fuxe J, Shoshan M. Repeated cisplatin treatment can lead to a multiresistant tumor cell population with stem cell features and sensitivity to 3-bromopyruvate. *Cancer Biol Ther* 2012;13:1454-62.
- (18) Mot AI, Liddell JR, White AR, Crouch PJ. Circumventing the Crabtree Effect: a method to induce lactate consumption and increase oxidative phosphorylation in cell culture. *Int J Biochem Cell Biol* 2016;79:128-38.
- (19) Sonveaux P, Vegran F, Schroeder T, Wergin MC, Verrax J, Rabbani ZN, et al. Targeting lactate-fueled respiration selectively kills hypoxic tumor cells in mice. *J Clin Invest* 2008;118:3930-42.
- (20) Sonveaux P, Brouet A, Havaux X, Gregoire V, Dessy C, Balligand JL, et al. Irradiation-induced angiogenesis through the up-regulation of the nitric oxide pathway: implications for tumor radiotherapy. *Cancer Res* 2003;63:1012-9.
- (21) Valente AJ, Maddalena LA, Robb EL, Moradi F, Stuart JA. A simple ImageJ macro tool for analyzing mitochondrial network morphology in mammalian cell culture. *Acta Histochem* 2017;119:315-26.
- (22) Rooney JP, Ryde IT, Sanders LH, Howlett EH, Colton MD, Germ KE, et al. PCR based determination of mitochondrial DNA copy number in multiple species. *Methods Mol Biol* 2015;1241:23-38.
- (23) Li H, Durbin R. Fast and accurate short read alignment with Burrows-Wheeler transform. *Bioinformatics* 2009;25:1754-60.
- (24) Van Hee VF, Perez-Escuredo J, Cacace A, Copetti T, Sonveaux P. Lactate does not activate NF-kappaB in oxidative tumor cells. *Front Pharmacol* 2015;6:228.

- (25) Xin L, Zhou Q, Yuan YW, Zhou LQ, Liu L, Li SH, et al. METase/lncRNA HULC/FoxM1 reduced cisplatin resistance in gastric cancer by suppressing autophagy. *J Cancer Res Clin Oncol* 2019;145:2507-17.
- (26) Benard G, Bellance N, James D, Parrone P, Fernandez H, Letellier T, et al. Mitochondrial bioenergetics and structural network organization. *J Cell Sci* 2007;120:838-48.
- (27) Kim I, Rodriguez-Enriquez S, Lemasters JJ. Selective degradation of mitochondria by mitophagy. *Arch Biochem Biophys* 2007;462:245-53.
- (28) Park S, Choi SG, Yoo SM, Son JH, Jung YK. Choline dehydrogenase interacts with SQSTM1/p62 to recruit LC3 and stimulate mitophagy. *Autophagy* 2014;10:1906-20.
- (29) Levy JMM, Towers CG, Thorburn A. Targeting autophagy in cancer. *Nat Rev Cancer* 2017;17:528-42.
- (30) Xu Y, Gao W, Zhang Y, Wu S, Liu Y, Deng X, et al. ABT737 reverses cisplatin resistance by targeting glucose metabolism of human ovarian cancer cells. *Int J Oncol* 2018;53:1055-68.
- (31) Zhang XY, Zhang M, Cong Q, Zhang MX, Zhang MY, Lu YY, et al. Hexokinase 2 confers resistance to cisplatin in ovarian cancer cells by enhancing cisplatin-induced autophagy. *Int J Biochem Cell Biol* 2018;95:9-16.
- (32) Dar S, Chhina J, Mert I, Chitale D, Buekers T, Kaur H, et al. Bioenergetic adaptations in chemoresistant ovarian cancer cells. *Sci Rep* 2017;7:8760.
- (33) Ricci F, Brunelli L, Affatato R, Chila R, Verza M, Indraccolo S, et al. Overcoming platinum-acquired resistance in ovarian cancer patient-derived xenografts. *Ther Adv Med Oncol* 2019;11:1758835919839543.

- (34) Payen VL, Zampieri LX, Porporato PE, Sonveaux P. Pro- and antitumor effects of mitochondrial reactive oxygen species. *Cancer Metastasis Rev* 2019;38:189-203.
- (35) Pasto A, Bellio C, Pilotto G, Ciminale V, Silic-Benussi M, Guzzo G, et al. Cancer stem cells from epithelial ovarian cancer patients privilege oxidative phosphorylation, and resist glucose deprivation. *Oncotarget* 2014;5:4305-19.
- (36) Ahmed N, Escalona R, Leung D, Chan E, Kannourakis G. Tumour microenvironment and metabolic plasticity in cancer and cancer stem cells: Perspectives on metabolic and immune regulatory signatures in chemoresistant ovarian cancer stem cells. *Semin Cancer Biol* 2018;53:265-81.
- (37) Roy L, Cowden Dahl KD. Can stemness and chemoresistance be therapeutically targeted via signaling pathways in ovarian cancer? *Cancers (Basel)* 2018;10.
- (38) Emmings E, Mullany S, Chang Z, Landen CN, Jr., Linder S, Bazzaro M. Targeting mitochondria for treatment of chemoresistant ovarian cancer. *Int J Mol Sci* 2019;20.
- (39) Kong B, Tsuyoshi H, Orisaka M, Shieh DB, Yoshida Y, Tsang BK. Mitochondrial dynamics regulating chemoresistance in gynecological cancers. *Ann N Y Acad Sci* 2015;1350:1-16.
- (40) Yu Y, Xu L, Qi L, Wang C, Xu N, Liu S, et al. ABT737 induces mitochondrial pathway apoptosis and mitophagy by regulating DRP1-dependent mitochondrial fission in human ovarian cancer cells. *Biomed Pharmacother* 2017;96:22-9.
- (41) Shen L, Sun B, Sheng J, Yu S, Li Y, Xu H, et al. PGC1alpha promotes cisplatin resistance in human ovarian carcinoma cells through upregulation of mitochondrial biogenesis. *Int J Oncol* 2018;53:404-16.

- (42) Kingnate C, Charoenkwan K, Kumfu S, Chattipakorn N, Chattipakorn SC. Possible roles of mitochondrial dynamics and the effects of pharmacological interventions in chemoresistant ovarian cancer. *EBioMedicine* 2018;34:256-66.
- (43) Jiang S, Chang H, Deng S, Fan D. Icariin enhances the chemosensitivity of cisplatinresistant ovarian cancer cells by suppressing autophagy via activation of the AKT/mTOR/ATG5 pathway. *Int J Oncol* 2019;54:1933-42.
- (44) Qiu S, Sun L, Zhang Y, Han S. Downregulation of BAG3 attenuates cisplatin resistance by inhibiting autophagy in human epithelial ovarian cancer cells. *Oncol Lett* 2019;18:1969-78.
- (45) Tan WX, Xu TM, Zhou ZL, Lv XJ, Liu J, Zhang WJ, et al. TRP14 promotes resistance to cisplatin by inducing autophagy in ovarian cancer. *Oncol Rep* 2019;42:1343-54.
- (46) Tang J, Zhu J, Ye Y, Liu Y, He Y, Zhang L, et al. Inhibition LC3B can increase chemosensitivity of ovarian cancer cells. *Cancer Cell Int* 2019;19:199.
- (47) You Y, Bi FF, Jiang Y, Xu YT, An YY, Li D, et al. BRCA1 affects the resistance and stemness of SKOV3-derived ovarian cancer stem cells by regulating autophagy. *Cancer Med* 2019;8:656-68.
- (48) Peng Q, Qin J, Zhang Y, Cheng X, Wang X, Lu W, et al. Autophagy maintains the stemness of ovarian cancer stem cells by FOXA2. *J Exp Clin Cancer Res* 2017;36:171.
- (49) Chen CD, Dai LN, Wang M, Lai XH, Wang J. Hypoxia induces autophagy in PA-I ovarian teratoma cells and resistance to growth inhibition and apoptosis by chemotherapeutic agent cis-diamminedichloroplatinum. *Eur J Gynaecol Oncol* 2017;38:277-81.

- (50) Long F, Liu W, Jia P, Wang H, Jiang G, Wang T. HIF-1alpha-induced autophagy contributes to cisplatin resistance in ovarian cancer cells. *Pharmazie* 2018;73:533-6.

Figures

Figure 1. Validation of isogenic models of cisplatin-sensitive and cisplatin-resistant human ovarian carcinoma cells. (A) SKOV-3 and SKOV-3-R cell numbers were determined by direct counting on a SpectraMax cytometer 24 h (*left graph*) and 48 h (*right graph*) after treatment with the indicated doses of cisplatin ($N = 3$, $n = 8-24$). (B) Clonogenic survival of the cells after a 48 h treatment with the indicated doses of cisplatin (*left graph*) and corresponding LC50s (*right graph*) ($N = 3$, $n = 5-15$). (C) As in (A) but using COV-362 and COV-362-R cells ($N = 2$, $n = 8$). (D) As in (B) but using COV-362 and COV-362-R cells ($N = 2$, $n = 4-9$). (E) Cells were treated for 48 h \pm 10 μ M of cisplatin, washed, and cultured for the indicated time in fresh medium without cisplatin. Graph shows SKOV-3 and SKOV-3-R (*left*, $N = 2$, $n = 8$) and COV-362 and COV-362-R (*right*, $N = 2$, $n = 8$) numbers over time determined during treatment recovery using crystal violet staining. (F) Mice were implanted either with SKOV-3 or with SKOV-3-R cells, and treated \pm 3 mg/kg of cisplatin every 3 days for 7 times (days 6 to 20). Graphs show tumor growth in mice (*left*) and tumor doubling times (*right*) ($n = 4-8$). (G) Mice were simultaneously implanted with SKOV-3 and SKOV-3-R cells in the left and right flanks, respectively, and treated \pm 3 mg/kg of cisplatin every 3 days (days 18 to 29). Graphs show tumor growth in mice (*left*) and tumor doubling times (*right*) ($n = 5-6$). Of note, SKOV-3-R cells did not generate tumors in the lifetime of these animals. * $P < 0.05$, *** $P < 0.005$, ns $P > 0.05$; by two-way ANOVA (A, C, E) with Sidak's (A, C) or Dunnett's (E) post-hoc test; by Student's t test (B *right*, D *right*, G *right*); and by one-way ANOVA with Dunnett's post-hoc test (F *right*).

Figure 2. Cisplatin-resistant human ovarian cancer cells undergo an oxidative switch. (A) Glucose consumption (*left graph*) and lactate production (*middle graph*) by SKOV-3 and SKOV-3-R cells in the absence of cisplatin was measured over 72 h on a CMA600 enzymatic analyzer. The right graph shows the lactate/glucose ratio in the cells ($N = 2$, $n = 5$). (B) Basal (*left graph*) and maximal (*right graph*) oxygen consumption rates (OCRs) of SKOV-3 and SKOV-3-R cells were measured on a Seahorse XF96 bioenergetic analyzer ($N = 3$, $n = 34-36$). (C) Glucose consumption (*left graph*) and lactate production (*middle graph*) by COV-362 and COV-362-R cells in the absence of cisplatin was measured over 48 h on a CMA600 enzymatic analyzer. The right graph shows the lactate/glucose ratio in the cells ($N = 2$, $n = 3-6$). (D) As in (B) but using COV-362 and COV-362-R cells ($N = 2$, $n = 10-15$). (E) Basal (*left graph*) and maximal (*right graph*) OCRs were measured 48 h after the treatment of SKOV-3 and SKOV-3-R cells with 10 μ M of cisplatin ($N = 3$, $n = 35-36$). (F) As in (G) but using COV-362 and COV-362-R cells treated with 5 μ M or 10 μ M of cisplatin ($N = 3$, $n = 12-24$). ** $P < 0.01$, *** $P < 0.005$, ns $P > 0.05$; by Student's t test (A-E); and by two-way ANOVA with Sidak's post-hoc test (F).

Figure 3. Different mitochondrial changes are associated to cisplatin resistance in human ovarian cancer cells. (A-D) SKOV-3 and SKOV-3-R cells were treated \pm 10 μ M of cisplatin for 48 h. (A) Representative pictures of the cells, where mitochondria are stained in green (TOMM20) and cell nuclei in blue (DAPI). Bar = 20 μ m. (B) Number of mitochondria individuals per cell ($N = 2$, $n = 8-12$). (C) Number of mitochondrial networks (*i.e.*, interconnected mitochondria with at least 2 branches) per cell ($N = 2$, $n = 8-12$). (D)

Mitochondrial surface per cell (μm^2) ($N = 2$, $n = 8-12$). (E) Mitochondrial DNA content normalized by nuclear DNA content in untreated cells ($N = 3$, $n = 6-9$). (F-I) COV-362 and COV-362-R cells were treated $\pm 10 \mu\text{M}$ of cisplatin for 48 h. (F) Representative pictures of COV-362 and COV-362-3-R cells $\pm 10 \mu\text{M}$ of cisplatin, where mitochondria are stained in green (TOMM20) and cell nuclei in blue (DAPI). Bar = 20 μm . (G) Number of mitochondria individuals per cell ($N = 1$, $n = 19-20$). (H) Number of mitochondrial networks per cell ($N = 1$, $n = 19-20$). (I) Mitochondrial surface per cell (μm^2) ($N = 1$, $n = 19-20$). (J) Mitochondrial DNA content normalized by nuclear DNA content in untreated cells ($N = 1$, $n = 2$). *** $P < 0.005$, *ns* $P > 0.05$ versus untreated sensitive cells; # $P < 0.05$, ## $P < 0.01$, *ns* $P > 0.05$ versus untreated resistant cells; by one-way ANOVA with Dunnett's post-hoc test (B-D, G-I) or by Student's *t* test (E, J).

Figure 4. Cisplatin-resistant human ovarian cancer cells bypass cisplatin-induced S-phase arrest despite equal DNA damage and independently of redox alterations.

(A) SKOV-3 and SKOV-3-R cells were treated $\pm 10 \mu\text{M}$ of cisplatin for the indicated times, after which the cell cycle was analyzed using propidium iodide in FACS assays. Representative graphs are shown, as well as the percentage of cells in each phase of the cycle ($N = 2-3$, $n = 2-4$). (B) The cells were treated $\pm 10 \mu\text{M}$ cisplatin for 48 h, after which the mean fluorescence intensity (MFI) of an antibody detecting cisplatin-DNA adducts was quantified using FACS ($N = 3$, $n = 3$). (C) Basal ROS content of SKOV-3 and SKOV-3-R cells measured with CM-H₂DCFDA ($N = 2$, $n = 2$). (D) The cells were treated for 48 h with 5 μM of H₂O₂, followed by a clonogenic assay ($N = 1$, $n = 3$). (E) SKOV-3 and SKOV-3-R cell numbers were determined 24 h (*left graph*) and 48 h (*right graph*) after treatment with the indicated doses of cisplatin. Where indicated, cells were pretreated for 72 h with *N*-acetyl-*L*-cysteine (NAC, 5 mM) ($N = 2$, $n = 8$). (F) Clonogenic assay of the cells after 72 h of pretreatment with 5 mM of NAC followed by a 48 h treatment with 10 μM of cisplatin ($N = 1$, $n = 3$). * $P < 0.05$, *** $P < 0.005$, *ns* $P > 0.05$; by Student's *t* test (B-D) or by two-way ANOVA (E, F) with Dunnett's post-hoc test (F).

Figure 5. Mitophagy is increased in cisplatin-resistant human ovarian cancer cells.

(A) SKOV-3 and SKOV-3-R cells were treated $\pm 10 \mu\text{M}$ of cisplatin for 48 h, after which LC3-I, LC3-II and β -actin expression was detected using western blotting. A representative picture is shown, and graphs show protein expression normalized to β -actin in untreated cells (*left*), cisplatin-treated cells (*middle*), and the LC3-II/LC3-I ratio in treated cells normalized by untreated cells (*right*) ($N = 2$, $n = 7-8$). (B) Where indicated, SKOV-3 and SKOV-3-R cells were treated for 48 h with bafilomycin A1 (10 nM), cisplatin (10 μM) or the combination of cisplatin (10 μM) and bafilomycin A1 (10 nM). Representative pictures are shown where mitochondria are stained in green (TOMM20), p62 in red and cell nuclei in blue (DAPI). Bar = 20 μm . The graph shows the percentage of mitochondria per cell that colocalize with p62 ($N = 1$, $n = 10-46$). (C) As in (B), but using COV-362 and COV-362-R cells. Bar = 20 μm . * $P < 0.05$, ** $P < 0.01$, *** $P < 0.005$, *ns* $P > 0.05$ versus untreated cisplatin-sensitive cells; # $P < 0.05$, ### $P < 0.005$, *ns* $P > 0.05$ versus untreated cisplatin-resistant cells; by Student's *t* test (A) or one-way ANOVA with Dunnett's post-hoc test (B, C).

Figure 6. (A) SKOV-3 (*left graph*) and SKOV-3-R (*right graph*) cells were treated for the indicated times \pm bafilomycin A1 (5 or 10 nM). Cell numbers were determined by direct

count on a SpectraMax cytometer ($N = 3$, $n = 16$). **(B)** As in (A), but using COV-362 (*left*) and COV-362-R (*right*) cells ($N = 1-2$, $n = 4-12$). **(C)** SKOV-3 and SKOV-3-R ($N = 3$, $n = 8-16$; *left*) and COV-362 and COV-362-R ($N = 2-3$, $n = 8-16$; *right*) cells were treated for the indicated times \pm cisplatin ($10 \mu\text{M}$) \pm bafilomycin A1 (10 nM). Cell numbers were determined by direct count on a SpectraMax cytometer. **(D)** Surviving fraction of a clonogenic assay of SKOV-3 *versus* SKOV-3-R ($N = 3$, $n = 9$; *left*) and COV-362 *versus* COV-362-R ($N = 2-3$, $n = 8-16$; *right*) cells after 48 h of treatment with 10 nM bafilomycin A1. *** $P < 0.005$, *ns* $P > 0.05$, by two-way ANOVA (A-C) or Student's *t* test (D).

Figure 1

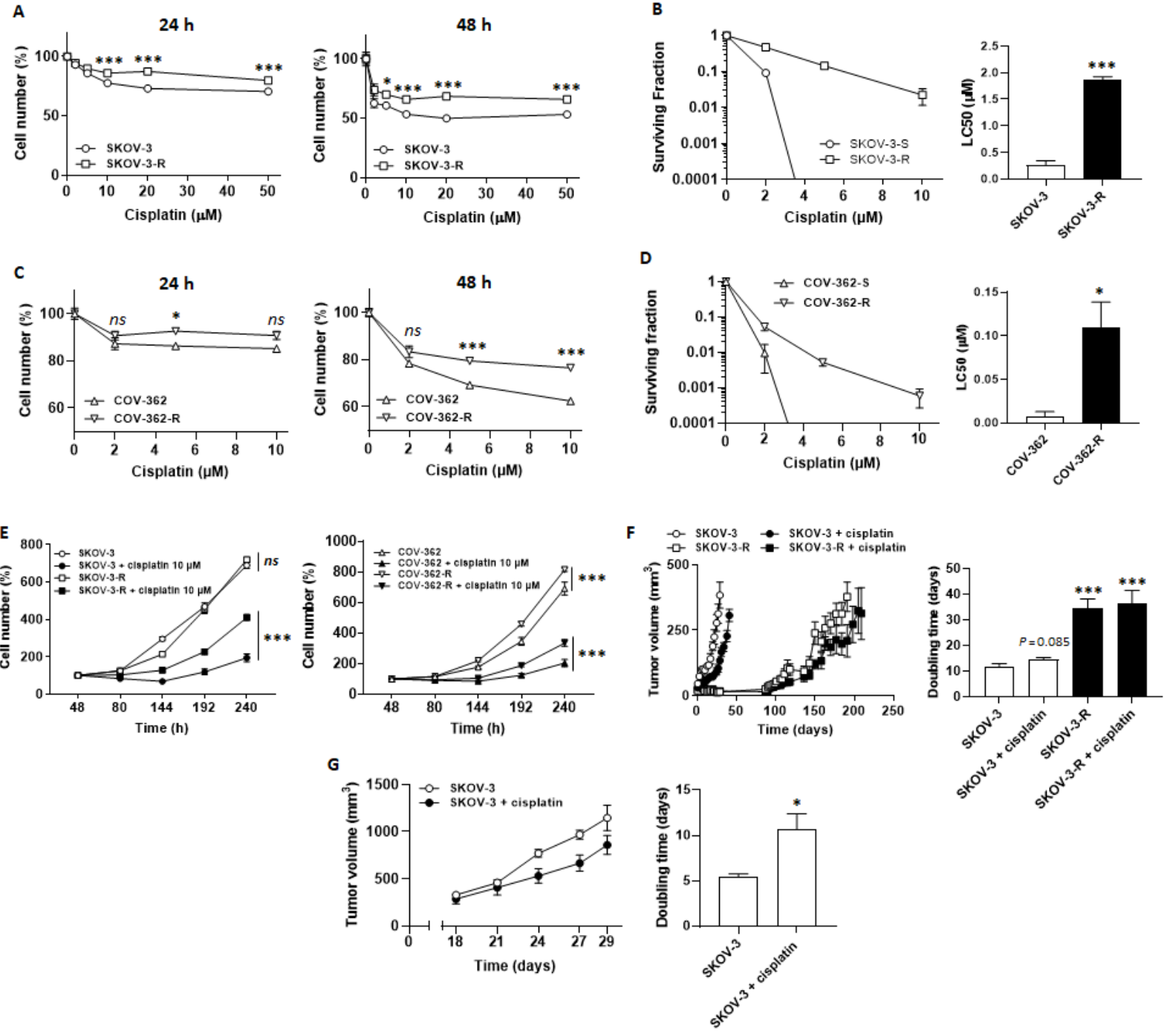


Figure 2

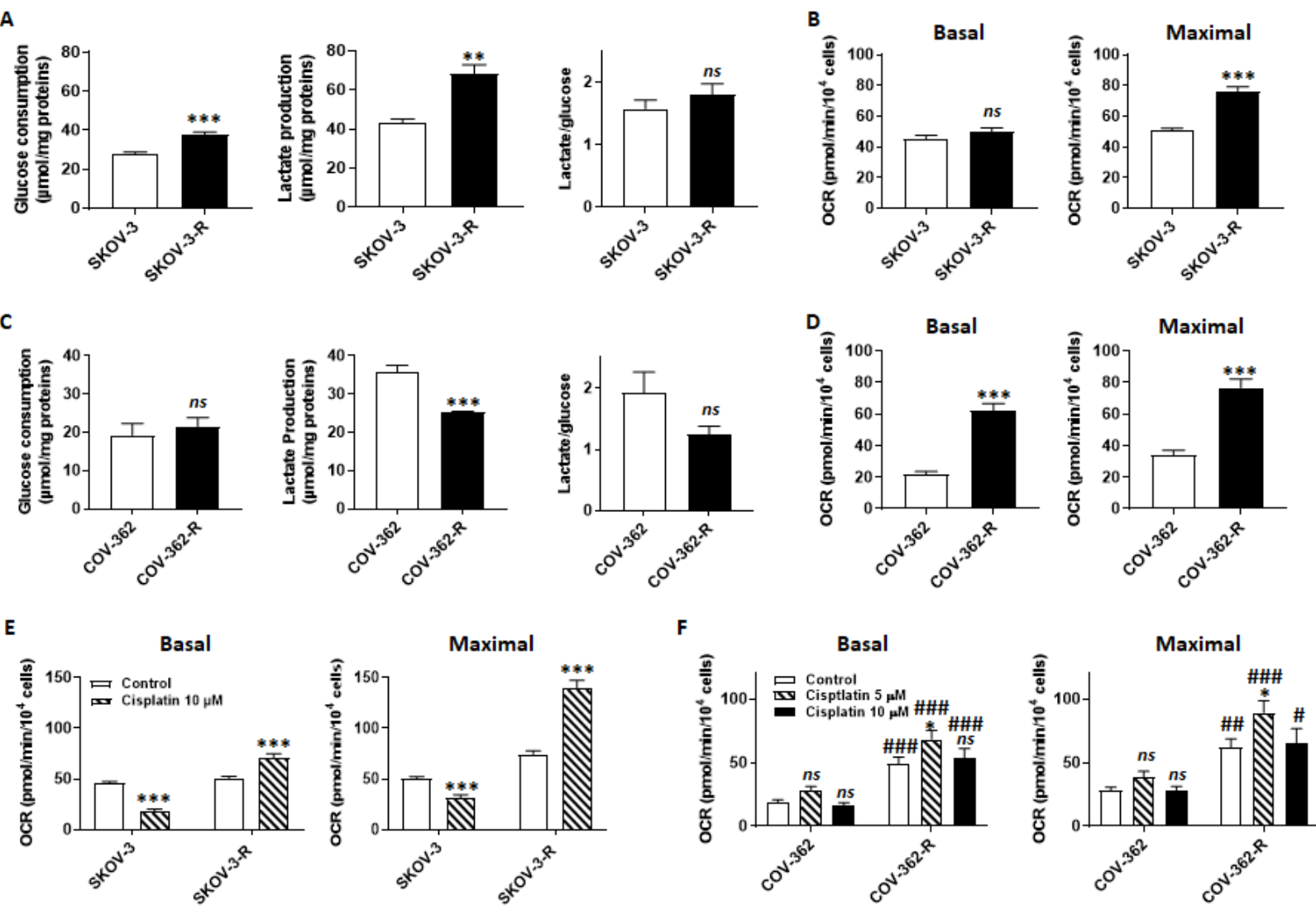


Figure 3

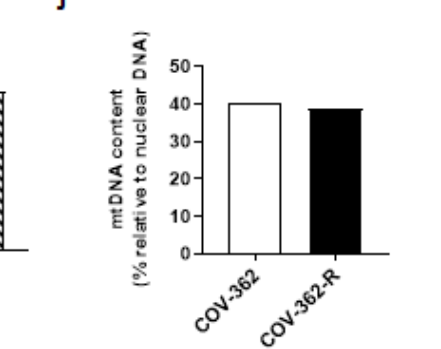
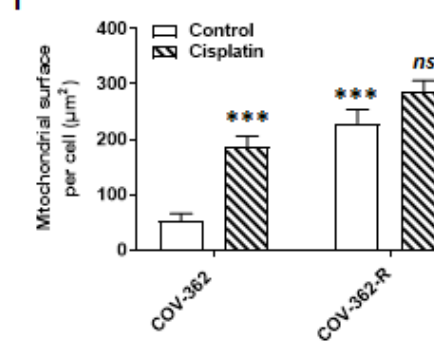
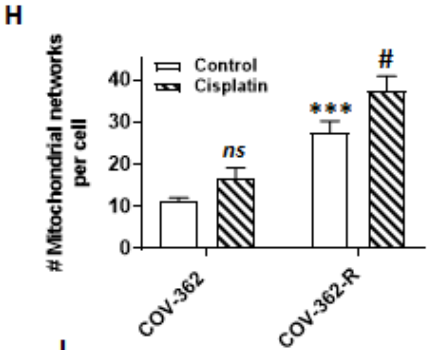
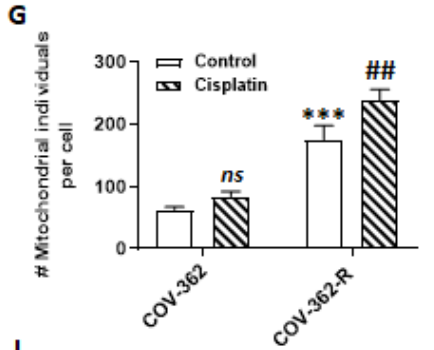
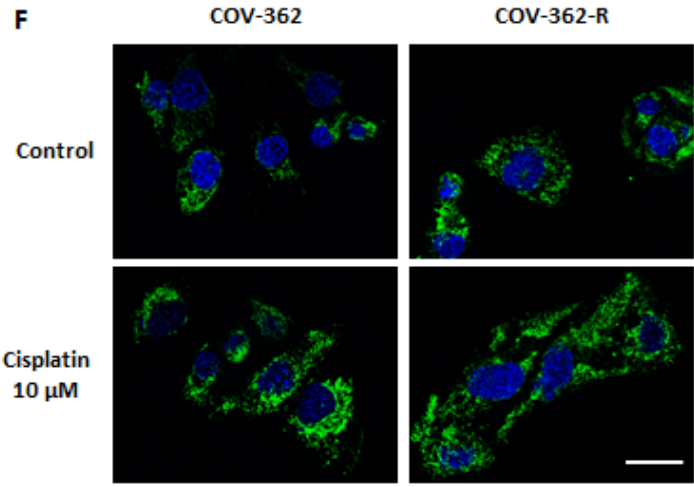
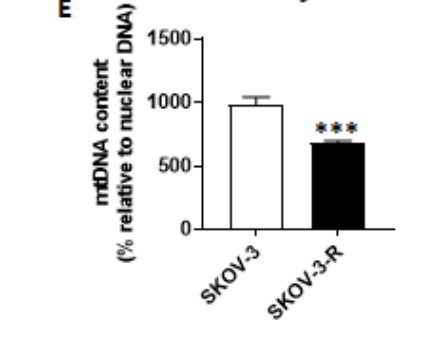
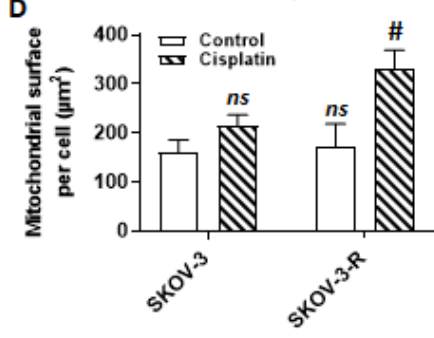
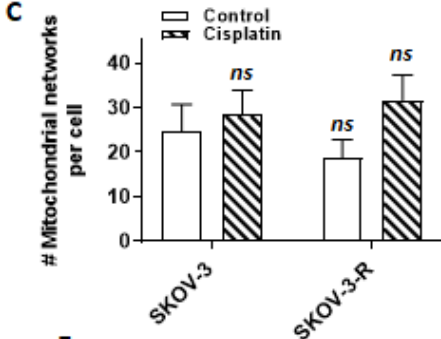
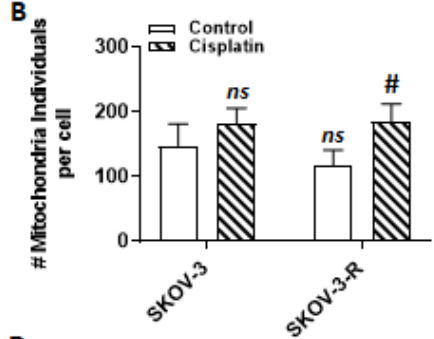
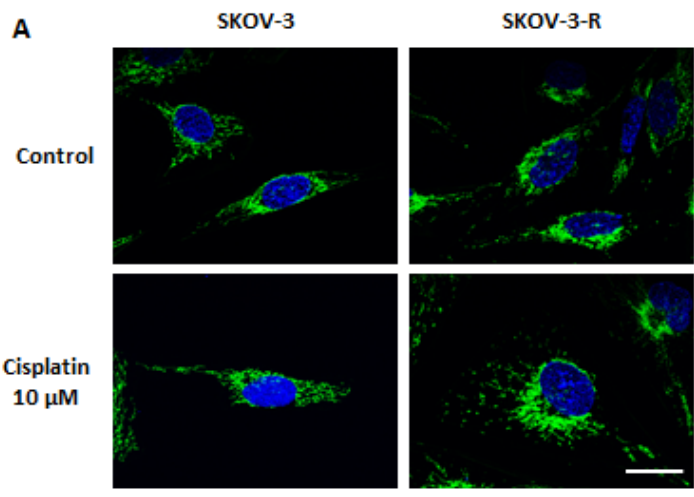


Figure 4

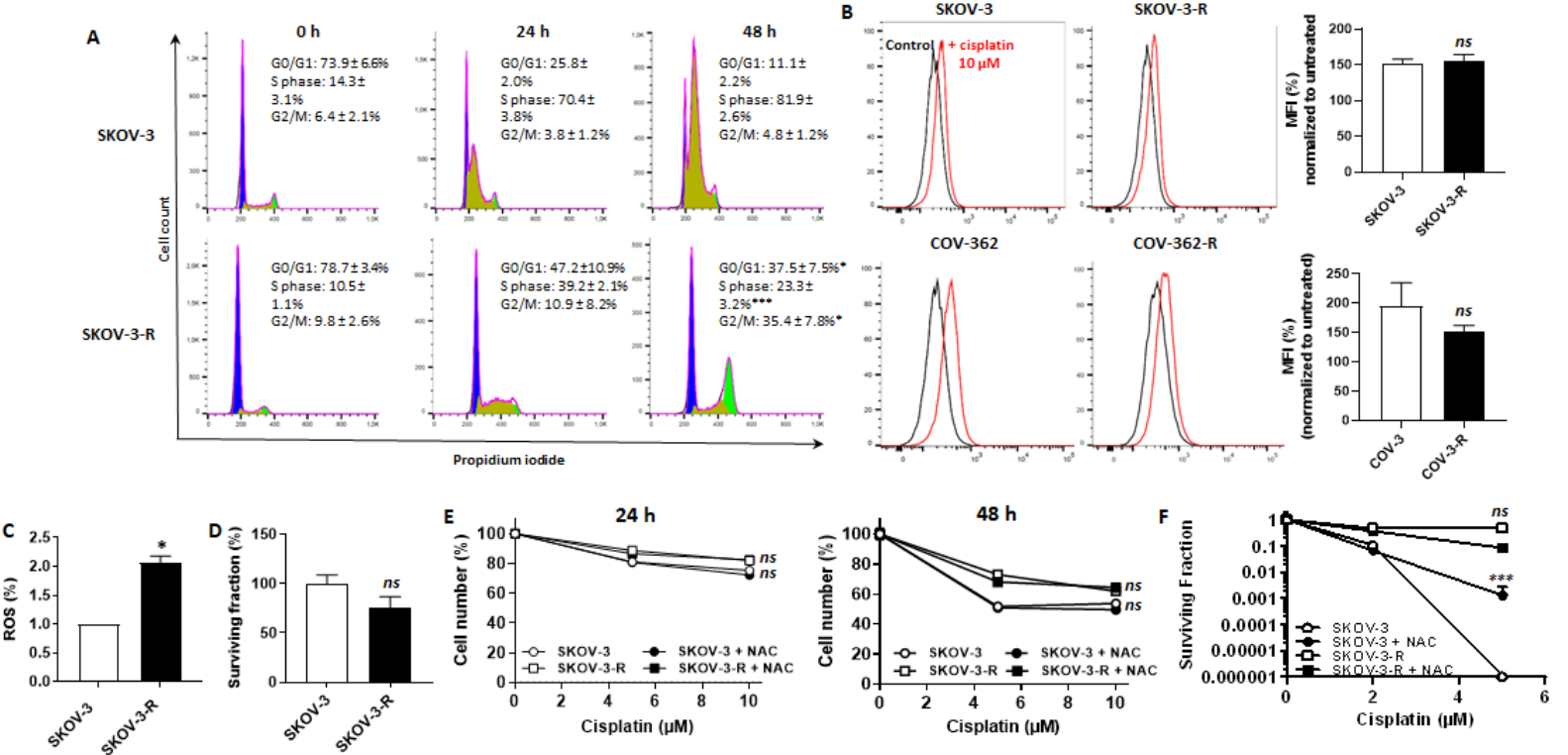


Figure 5

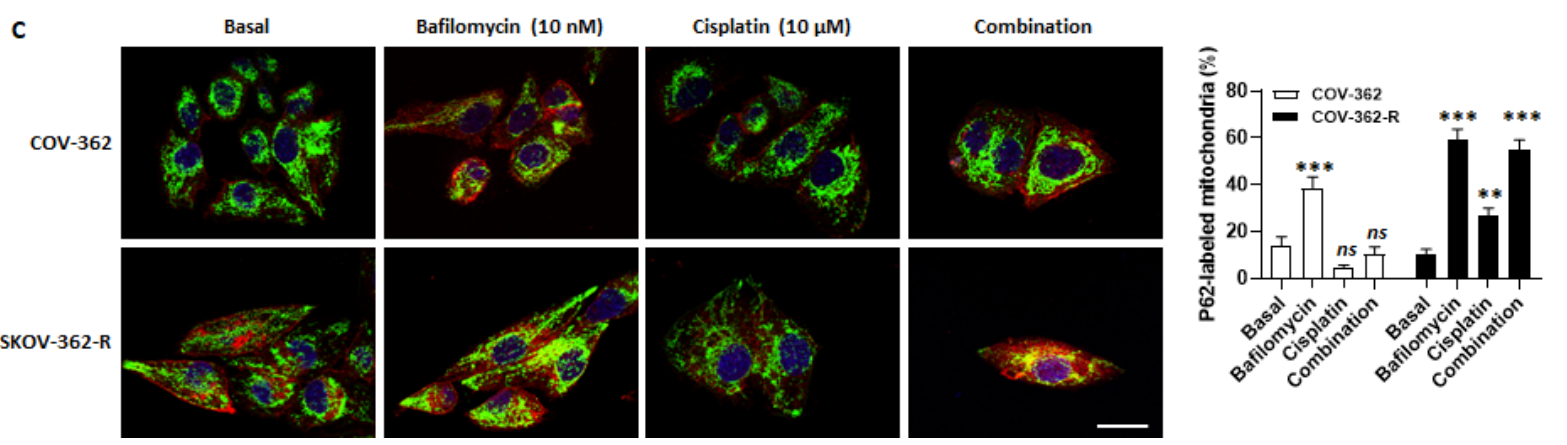
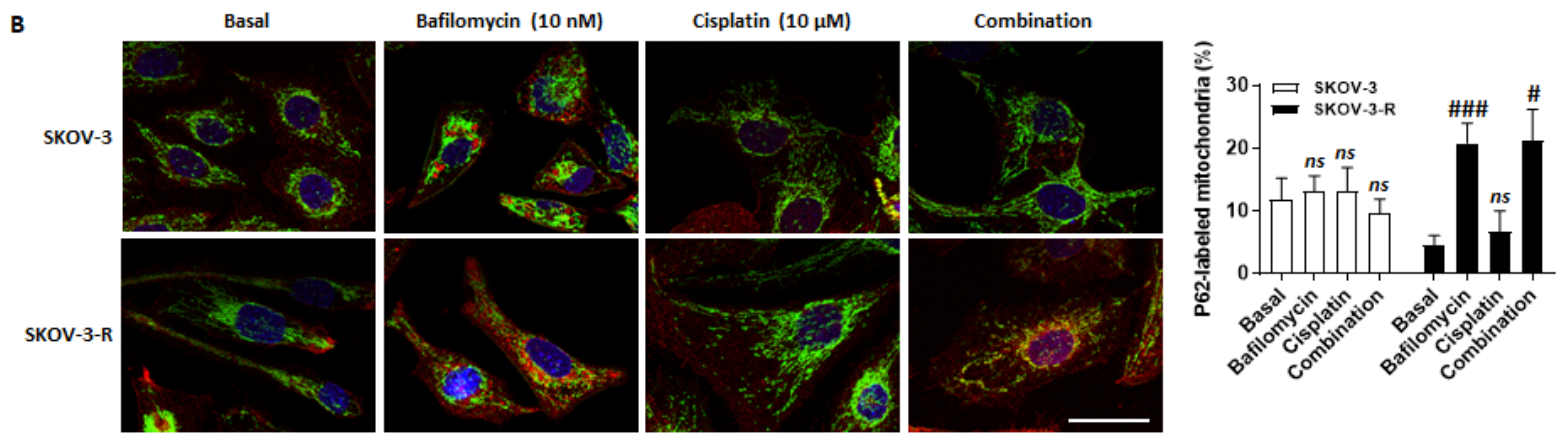
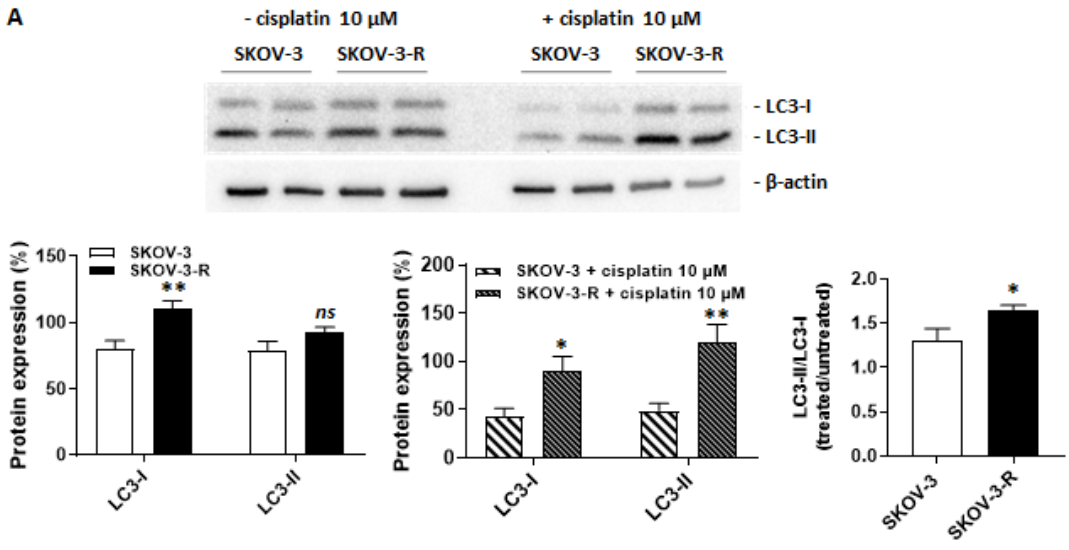


Figure 6

